npj | Quantum Information

ARTICLE   OPEN

Squeezing and quantum state engineering with Josephson travelling wave amplifiers

Arne L. Grimsmo[1] and Alexandre Blais[1,2]

We develop a quantum theory describing the input–output properties of Josephson traveling wave parametric amplifiers. This allows us to show how such a device can be used as a source of nonclassical radiation, and how dispersion engineering can be used to tailor gain profiles and squeezing spectra with attractive properties, ranging from genuinely broadband spectra to "squeezing combs" consisting of a number of discrete entangled quasimodes. The device's output field can furthermore be used to generate a multi-mode squeezed bath—a powerful resource for dissipative quantum state preparation. In particular, we show how it can be used to generate continuous variable cluster states that are universal for measurement based quantum computing. The favorable scaling properties of the preparation scheme makes this a promising path towards continuous variable quantum computing in the microwave regime.

INTRODUCTION

Microwave quantum optics is an emerging field where artificial atoms, such as quantum dots,[1] spin ensembles[2] or superconducting quantum circuits[3] are placed in engineered electromagnetic environments. Strong light–matter interaction can be achieved by confining the electromagnetic field in microwave resonators[3, 4] or one-dimensional waveguides.[5, 6] The flexibility offered by microwave engineering allows experimentalists to go beyond the limits of conventional quantum optics in many ways. Examples include reaching the so-called ultrastrong coupling regime of light–matter interaction,[7] and using nonlinear microwave resonators to simulate relativistic quantum effects.[8]

A recent advancement in microwave quantum optics is the bottom-up design of nonlinear, one-dimensional metamaterials with strong photon–photon interactions and engineered dispersion relations.[9–11] The nonlinearity in these metamaterials is provided by Josephson junctions embedded in a transmission line, with photon–photon interactions activated by a strong pump tone through a parametric four-wave mixing process. These devices have been dubbed Josephson travelling wave parametric amplifiers (JTWPAs),[10] and are analogous to one-dimensional $\chi^{(3)}$ nonlinear crystals.[12]

The development of JTWPAs is motivated by their potential use as amplifiers for readout of solid-state qubits. The extremely high measurement fidelity necessary for fault-tolerant quantum computing requires amplifiers with added noise near the fundamental quantum limit.[13, 14] A key advantage to the JTWPA design is the operational bandwidth, which is in the GHz range. This is in contrast to other near-quantum-limited microwave amplifiers based on resonant cavity interactions, which typically have bandwidths of a few tens of MHz.[15–17] An amplifier operating near the quantum limit is, however, very different from a classical amplifier. In particular, quantum-limited phase preserving amplification implies the presence of entanglement between the amplified signal and an "idler" signal in a two-mode squeezed state.[13, 18] This motivates an alternative viewpoint on the JTWPA: besides using the device to amplify a signal of interest, it can also be viewed as a source of nonclassical radiation. The large bandwidth and simple on-chip integration with coherent quantum systems, such as superconducting qubits and microwave resonators, makes the JTWPA an intriguing new resource for generating quantum radiation with potential applications in metrology and quantum information processing, amongst others.[19–26]

In this paper, we show how the inherent flexibility in the bottom-up JTWPA construction allows us to tailor the quantum properties of the output field leaving the device. In particular, we show how to shape the profile of the broadband squeezing spectrum of the output field, and how to cut holes in this spectrum such that some frequency ranges are unaffected by the nonlinear interaction. This type of spectrum engineering is useful for applications of squeezing to quantum informaton processing tasks, for example to avoid unwanted quantum heating.[27]

We subsequently demonstrate how the JTWPA can be used as a resource for dissipative quantum state preparation. Dissipative quantum state preparation has over the last years emerged as an alternative to preparation of entangled states using coherent Hamiltonian[28] or gate-based methods.[29] It has been shown that universal quantum computing can be achieved through dissipative processes alone[30] and, in a similar vein, that highly correlated states, such as stabilizer states and projected entangled pair states can be created as stable steady states of dissipative processes.[30, 31] In this paper, we show that broadband squeezed radiation, such as the radiation emitted by a JTWPA, is a particularly potent resource for dissipative quantum state preparation. The emitted radiation generates a multimode squeezed vacuum, which can be used to drive quantum systems placed at the source's output into entangled states through correlated photon absorption and emission processes. We show that by engineering such a

[1]Institut quantique and Départment de Physique, Université de Sherbrooke, Sherbrooke J1K 2R1 QC, Canada and [2]Canadian Institute for Advanced Research, Toronto, ON, Canada
Correspondence: Arne L. Grimsmo (arne.grimsmo@gmail.com)

npj nature partner journals

squeezed bath, one can produce pairs of entangled qubits as well as continuous variable (CV) cluster states—the latter being universal resource states for measurement-based quantum computing. The preparation schemes are simple, requiring no Hamiltonian interactions or complicated reservoir engineering. By exploiting the large bandwidth of the JTWPA, the process can furthermore be implemented in a very hardware-efficient manner.

The purely dissipative nature of the preparation process distinguishes our proposal from similar approaches for generating cluster states in the optical regime.[32–37] A distinct advantage of a dissipative scheme is that it relaxes constraints on locality, which might allow for a more modular architecture that avoids spurious interactions and increases scalability.[38]

Although we focus on JTPWAs as squeezing sources in this work, due to their design flexibility and large bandwidth, we emphasize that the dissipative quantum state preparation schemes we develop are relevant for any type of broadband squeezing source that can be integrated with coherent quantum systems, such as other types of traveling wave amplifiers,[39, 40] impedance engineered Josephson parametric amplifiers,[41] squeezing sources based on reservoir engineering,[42] or the nonclassical radiation emitted by an ac-biased tunnel junction.[43, 44]

RESULTS

To describe the JTWPA's squeezing properties, we first need a quantized theory of its dynamics. Classical treatments of a JTWPA are presented in refs 9, 11, 45. In the following, we give a Hamiltonian treatment of the nonlinear dynamics, taking into account dispersion and the continuum nature of the electromagnetic field in the waveguide.

The device we consider in this paper is depicted in Fig. 1. It consists of a series of identical coupled Josephson junctions with Josephson energies E_J and junction plasma frequencies ω_p. Each junction is coupled to ground by a passive, dissipationless element with impedance $Z(\omega)$, which is left arbitrary for now. By engineering $Z(\omega)$ one can modify the dispersion relation of waves propagating through the device as shown in ref. 9. We show below how this can be used to tailor the squeezing properties of the output field leaving the device. Note that other variants of the JTWPA device where the Josephson junctions are replaced by SQUIDs have recently been discussed.[46, 47] We do not consider such modifications here, but the general approach we develop below can be used to formulate a quantum theory also in these cases.

In experimental realizations, JTWPAs have several thousand junctions with a unit cell distance much smaller than the relevant wavelengths.[10, 11] One can therefore approximate the device with a continuum description (formally taking the unit cell distance, a, to zero). We furthermore assume that the JTWPA is coupled to identical, semi-infinite and impedance matched transmission lines to the left and the right, and we neglect any reflection of the field at the interfaces between the different sections.

As shown in detail in Supplemental Methods 1, a continuum limit Hamiltonian for the system can be written $\hat{H} = \hat{H}_0 + \hat{H}_1$, where $\hat{H}_0$ is a linear contribution containing all terms up to second order in the fields, and $\hat{H}_1$ is a nonlinear contribution due to the Josephson junction potential. The linear Hamiltonian can be diagonalized in terms of a set of frequency modes, following an approach introduced by Santos and Loudon in ref. 48, leading to the form

$$\hat{H}_0 = \sum_{\nu=\mathrm{L,R}} \int_0^\infty \mathrm{d}\omega\, \hbar\omega\, \hat{a}_{\nu\omega}^\dagger \hat{a}_{\nu\omega}, \tag{1}$$

where $[\hat{a}_{\nu\omega}, \hat{a}_{\mu\omega'}^\dagger] = \delta_{\nu\mu}\delta(\omega - \omega')$, and we have omitted the zero-point energy. The label $\nu \in \{\mathrm{L,R}\}$ labels left- and right-moving modes, respectively.
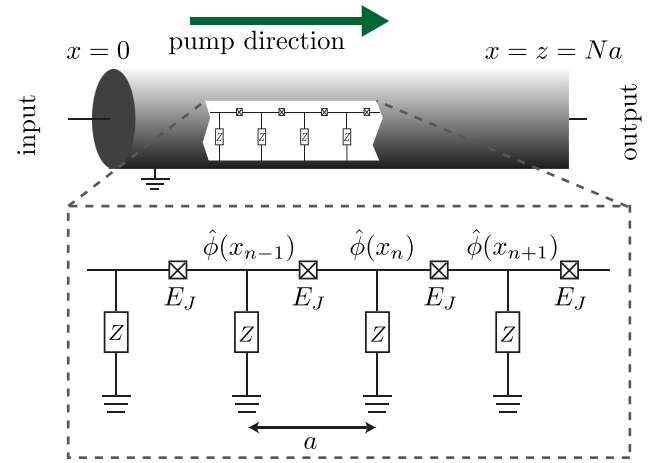

Fig. 1 Josephson traveling wave parametric amplifier. A chain of identical coupled Josephson junctions, with Josephson energy E_J and plasma frequency ω_p, are coupled in series. Each junction is furthermore coupled to ground by a passive, dissipationless element described by an impedance $Z(\omega)$. By designing this impedance one can engineer the dispersion relation for waves traveling through the device. A strong right-moving pump actives a four-wave mixing process through the Josephson potential, which can be used to generate squeezed light

For the nonlinear Hamiltonian, we systematically perform a series of approximations that are ultimately analogous to those used in the classical treatment given in refs 9, 11, 45. A quantized analog of the classical equation of motion found in previous work is shown to be a limiting case of a more general theory. As detailed in Methods, for a classical right-moving monochromatic pump at a frequency Ω_P, and neglecting terms that are smaller than second order in the pump, we can write the non-linear Hamiltonian in terms of three distinct contributions

$$\hat{H}_1 = \hat{H}_{\mathrm{CPM}} + \hat{H}_{\mathrm{SQ}} + H_{\mathrm{SPM}}, \tag{2}$$

where $\hat{H}_{\mathrm{CPM}}$ describes cross-phase modulation due to the pump, $\hat{H}_{\mathrm{SQ}}$ describes broadband squeezing, and H_{SPM} is a classical Hamiltonian describing self-phase modulation of the pump. Explicit expressions for these three Hamiltonians in terms of the frequency modes $\hat{a}_{\nu\omega}$ are given in Methods.

As shown in Methods, we find in a scattering limit where the initial and final times of the problem are taken to minus and plus infinity, respectively; the following is the expression for the asymptotic Heisenberg picture output field

$$\hat{a}_{R\omega}^{\mathrm{out}} = e^{i\left[2|\beta|^2 k_\omega + \Delta k(\omega)/2\right]z}\left[u(\omega,z)\hat{a}_{R\omega} + iv(\omega,z)\hat{a}_{R(2\Omega_p-\omega)}^\dagger\right], \tag{3}$$

where the functions $u(\omega, z)$ and $v(\omega, z)$, defined in Eqs. (28) and (29), satisfy $|u(\omega,z)|^2 - |v(\omega,z)|^2 = 1$, and

$$\Delta k(\omega) = 2k_p - k_\omega - k_{2\Omega_p-\omega} + 2|\beta|^2\left(k_p - k_{2\Omega_p-\omega} - k_\omega\right), \tag{4}$$

is the phase mismatch, including a nonlinear correction due to to the cross- and self-phase modulation of the pump. Here, k_ω is the wave-vector, which due to dispersion inside the JTWPA section has a non-linear dependence on ω:

$$k_\omega = \sqrt{\frac{-i\omega z^{-1}(\omega)l}{1 - \omega^2/\omega_P^2}}, \tag{5}$$

where l is the inductance per unit length of the JTWPA section, ω_P is the junction plasma frequency and $z^{-1}(\omega) = Z^{-1}(\omega)/a$ is the admittance to ground per unit cell. The parameter $\beta = I_p/4I_c$ in Eq. (4) is the dimensionless amplitude of the classical pump,
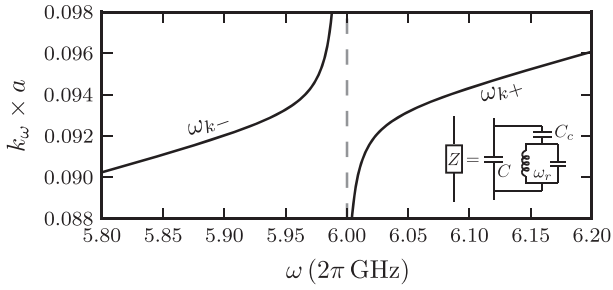
Fig. 2 Engineered bandgaps. Illustration of the disperion relation when $Z(\omega)$ (illustrated in the inset) describes a single resonant mode at a frequency ω_r linearly coupled to the flux field in every unit cell. A bandgap opens up around the resonance frequency, close to 6 GHz in this example. The width of the bandgap is set by the coupling capacitance C_c shown in the inset

expressed in units of the Josephson junction critical current I_c (see Methods for further details). As Eq. (5) clearly shows, the dispersion relation, and consequently the phase mismatch, can be tuned by engineering the admittance to ground in the JTWPA unit cells. In particular, if the impedance $Z(\omega)$ describes a resonant mode, a bandgap will open close to the resonance frequency. The behavior of the dispersion relation close to a bandgap is illustrated in Fig. 2. Note that if dispersion is neglected, $\Delta k(\omega) = 0$, Eq. (3) reduces to the standard input–output relation for a lossless parametric amplifier (see, e.g., ref. 49).

Engineering nonclassical radiation

The quantum input–output theory developed above allows us predict features of the JTPWA's output field, such as the device's gain profile and output field squeezing spectrum. In this section, we show how output spectra can be tailored through dispersion engineering. We focus first on an ideal, quantum-limited device and discuss the effect of loss below.

From Eq. (3), the JTWPA's amplitude gain is given by $u(\omega, z)$, and we define the power gain as $G(\omega, z) = |u(\omega, z)|^2$ refs 9, 13, 45. This function grows exponentially with z for small phase mismatch, $\Delta k(\omega) \simeq 0$, but is only of order one if the phase mismatch is large (see ref. 9 and Methods). The squeezing of the JTWPA's output field is manifested in correlations between frequencies ω and $2\Omega_P - \omega$, symmetric around the pump frequency. We define the squeezing spectrum of the device as[50]

$$S_R(\omega, z) = \int_0^\infty d\omega' \langle \Delta \hat{Y}_{R\omega}^\theta \Delta \hat{Y}_{R\omega'}^\theta \rangle$$

$$= 2N_R(\omega, z) + 1 - 2|M_R(\omega, z)|, \quad (6)$$

where we have defined quadratures $\hat{Y}_{R\omega}^\theta = i[e^{i\theta/2}\hat{a}_{R\omega}^{out\dagger} - e^{-i\theta/2}\hat{a}_{R\omega}^{out}]$, with fluctuations $\Delta \hat{Y}_{R\omega} = \hat{Y}_{R\omega} - \langle \hat{Y}_{R\omega} \rangle$ and θ the squeezing angle. The parameters $N_R(\omega, z)$ and $M_R(\omega, z)$ introduced on the right hand side of Eq. (6), are defined in Eqs. (31) and (32) and can be interpreted as the thermal photon number and a squeezing parameter for the right-moving field, respectively.

The gain and the squeezing at the output depends strongly on the phase mismatch $\Delta k(\omega)$. The phase mismatch can, however, be compensated for by tuning $Z(\Omega_P)$, as this allows for tuning the pump wavevector $k_p = k_{\Omega_p}$ according to Eq. (5). As was proposed theoretically in ref. 9 and demonstrated experimentally in refs. 10, 11, it is possible to tune the phase mismatch to zero at the pump frequency, $\Delta k(\Omega_P) \simeq 0$, and greatly reduce it across the whole JTWPA bandwidth. This is done by placing LC (or transmission line) resonators with resonance frequency $\omega_{r0} \simeq \Omega_P$ regularly
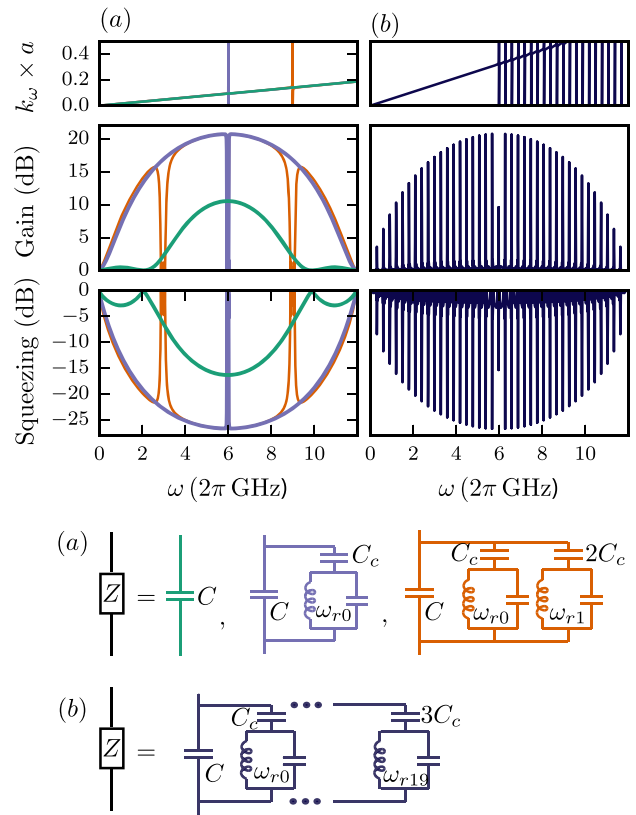

Fig. 3 Gain profile and squeezing spectra. Output field properties of a JTWPA with 2000 unit cells and parameters given in the text. **a** The *green lines* are for a device without RPM. The *blue lines* are for a device with identical parameters, but where RPM has been used to tune $\Delta k(\Omega_p) \simeq 0$. The *orange lines* show a device where in addition to RPM, a second resonance has been placed at 9 GHz punching two symmetric holes in the gain and squeezing spectra. **b** A JTWPA with 19 additional resonances used to generate a "squeezing comb." The choice of impedance to ground for each simulated device is illustrated below with color codes corresponding to the plots

along the JTWPA transmission line, a technique referred to as resonant phase matching (RPM).[9]

The effect of RPM on the gain and squeezing spectra is illustrated in Fig. 3 for a simulated device similar to what has been realized experimentally in refs 10, 11: The device length was chosen to be 2000 unit cells with characteristic impedance $Z_0 = 50\Omega$, critical current $I_c = (2\pi/\Phi_0)E_J = 2.75 \mu A$, dimensionless pump strength $\beta = 0.125$ and pump frequency $\Omega_p/2\pi = 5.97$ GHz. The ratio of the pump frequency to the junction plasma frequency was $\Omega_p/\omega_p = 8.2 \times 10^{-2}$. The *green lines* in Fig. 3a show the gain profile and squeezing spectrum of the output field for the device without RPM, while the *blue lines* show results for an identical device where RPM has been used to tune $\Delta k(\Omega_p) = 0$. The circuit parameters for the LC resonator are $C_c = 10$ fF, $C_r = 7.0$ pF, $L_r = 100$ pH, giving a resonance frequency of $\omega_{r0}/2\pi = 6.0$ GHz.

Two-mode squeezing has applications for entanglement generation,[19, 20] quantum teleportation,[21] interferometry,[22] creation of quantum mechanics free subsystems,[23] high-fidelity qubit readout[24, 25] and logical operations,[26] amongst others. A broadband squeezing source such as the JTWPA has a great advantage for scalability, as tasks can be parallelized with many pairs of far-separated two-mode squeezed frequencies using a single device. It is, however, not necessarily desirable to have squeezing at all frequencies over the operational bandwidth as this might lead, e.g., to unwanted quantum heating.[25, 27]
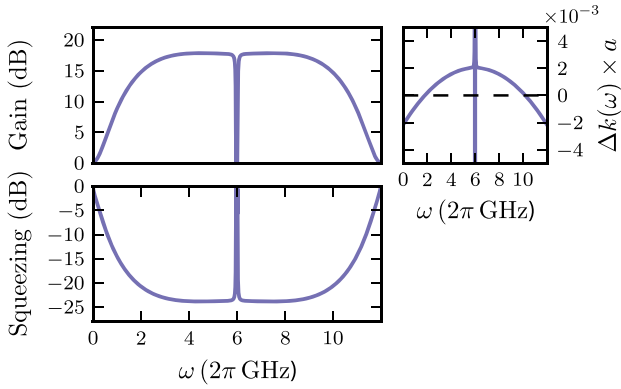
Fig. 4 Engineering flat spectra. A device similar to those in Fig. 3, but where RPM has been used to tune $\Delta k(\omega) = 0$ for $\omega/(2\pi) \simeq 1.8$ GHz. The larger phase mismatch around $\omega \simeq \Omega_p$, shown in the right panel, gives a flatter profile for both the gain and squeezing spectra

Building on the RPM technique, we consider placing additional resonances in each unit cell with resonance frequencies ω_{rk} away from Ω_P. This leads to a bandgap and a divergence in $k(\omega)$ close to each resonance ω_{rk}, as illustrated in Fig. 2. The huge phase mismatch close to these resonances prohibits any parametric interaction at $\omega \simeq \omega_{rk}$ and $\omega \simeq 2\Omega_p - \omega_{rk}$, effectively punching two symmetric holes in the gain and squeezing spectra. This is illustrated by the *orange lines* in Fig. 3a, where a single additional resonace has been placed at $\omega_{r1} = 9.0 \times 2\pi$ GHz. The parameters are otherwise as before, except that the second LC resonator is chosen to have twice the coupling capacitance, $2C_c$. This choice serves to illustrate how the width of the hole in the spectrum is determined by the coupling capacitance to the resonator, as is clearly seen when comparing the holes at ω_{r0} and ω_{r1}.

In Fig. 3b, we demonstrate how this technique can be used to engineer a "squeezing comb" where there is considerable gain and squeezing only for a discrete set of narrow quasimodes. With a larger number of closely spaced resonance frequencies—either using individual lumped LC circuits or the resonances of a multi-mode transmission line resonator—it is possible to have phase matching only over narrow frequency bandwiths. In Fig. 3b, we show the gain profile and squeezing spectrum where 19 additional resonances at $\omega_{rk} = \omega_{r0} + k \times \omega_{r0}/20$, $k = 1, 2, \ldots, 19$ has been used to create a squeezing comb with 38 quasimodes. Slightly different parameters were chosen for this device, to get similar gain and squeezing profiles as before: $Z_0 = 14\Omega$, $I_0 = 2.75\,\mu A$, $\beta = 0.069$, while the additional coupling capacitances were chosen to be $3.0C_c$. Note that it is not necessary to place the LC resonators in every unit cell in an experiment. In practice, RPM has been realized by repeatedly placing identical LCs every few unit cells.[10]

For certain applications, it might also be of interest to have a squeezing spectrum with a flatter profile than what is shown in Fig. 3. This can be achieved by suitably engineering the phase mismatch. In Fig. 4, we show a device where RPM has been used to tune $\Delta k(\omega) = 0$ for $\omega/2\pi \simeq 1.8$ GHz, with the pump frequency close to the resonance frequency at $\omega_{r0}/2\pi = 6$ GHz. The simulated device otherwise has parameters $Z_0 = 60\Omega$, $I_0 = 1.75\,\mu A$, $\beta = 0.113$. This choice of dispersion engineering leads to larger phase mismatch in the center region of the spectrum, close to the pump, giving the flatter profile shown in the figure.

Reduction in squeezing due to loss

Internal loss in the JTWPA, as well as insertion loss, is likely to be a source of reduction in squeezing from the ideal results shown in Fig. 3. A simplified loss model is a beam splitter with transmittance $\sqrt{\eta(\omega)}$ placed after the JTPWA, with vacuum noise incident on the beam splitter's second input port.[51] This leads to a reduction in
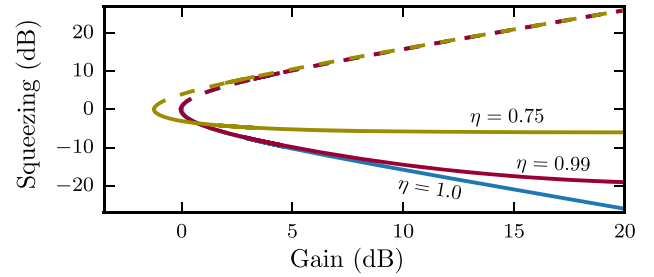

Fig. 5 Squeezing in the presence of loss. Squeezing as a function of gain, $G(\omega, z) = \eta |u(\omega, z)|^2$, in the presence of loss, modeled as a beam splitter with transmittance η placed at the JTWPA output. The *solid lines* show the maximally squeezed quadrature for three different values of η, while the *dashed lines* show the corresponding anti-squeezed quadrature

photon number, $N_R(\omega, z) \rightarrow |\eta(\omega)| N_R(\omega, z)$, and squeezing parameter, $M_R(\omega, z) \rightarrow \sqrt{\eta(\omega)}\sqrt{\eta(2\Omega_p - \omega)} M_R(\omega, z)$. Taking $\eta = \eta(\omega)$ frequency independent for simplicity, this gives a reduction in squeezing, $S_R(\omega, z) \rightarrow 2|\eta| N_R(\omega, z) + 1 - 2|\eta| |M_R(\omega, z)|$. Note that distributed loss throughout the JTWPA can be taken into account through a simple phenomenological model,[49] but this is beyond the scope of the present discussion.

Figure 5 shows the maximum squeezing level as a function of gain as the pump strength is ramped up. The parameters are otherwise identical to those used for the *blue lines* displayed in Fig. 3a. The *solid lines* show the maximally squeezed quadrature, while the *dashed lines* show the corresponding anti-squeezed quadrature, for three different values $\eta = 0.75$ (*yellow*), 0.99 (*dark red*) and 1.00 (*blue*). Note that the gain is also reduced by the loss, $G(\omega, z) = \eta |u(\omega, z)|^2$, such that we have attenuation at zero pump power.

For a non-unity η, the squeezing level saturates with gain, while the anti-squeezed quadrature keeps growing proportionally. The maximal squeezing depends sensitively on η: while a quantum-limited device with $\eta = 1$ would produce more than 25 dB of squeezing at 20 dB of gain, a device with $\eta = 0.75$ only gives about 6.5 dB of squeezing for the same gain. For a realistic device, further reductions in squeezing might arise due to disorder, the distributed nature of loss throughout the device, and the frequency dependence of the attenuation leading to asymmetry between the signal and idler [Kamal, A. Private communication (2016)].

Probing the output

The examples discussed above demonstrate how the flexible JTWPA design allows for generating nonclassical light with interesting and useful squeezing spectra.

The squeezing spectrum can be found experimentally by measuring the variance of filtered two-mode quadratures (see Supplemental Methods 1 and, e.g., refs. 43, 52–54). However, this necessarily includes insertion loss and noise from subsequent parts of the amplification chain,[10] which can make the detection of two-mode squeezing challenging. For a more direct probing of the JTWPA's performance, we propose placing two superconducting qubits capacitively coupled directly to the transmission line at the output port.

For two off-resonant qubits with respective frequencies $\omega_1 \neq \omega_2$, and $\omega_1 + \omega_2 \neq 2\Omega_p$, the qubits will be in uncorrelated thermally populated states. If, however, $\omega_1 + \omega_2 = 2\Omega_p$, the qubits become entangled and information about the JTWPA's squeezing spectrum is encoded in the joint two-qubit density matrix. This information can then be extracted by measuring qubit–qubit correlation functions.

Assuming for simplicity a single right-moving pump and a left-moving field in the vacuum state, we have that for $\omega_1 + \omega_2 \neq 2\Omega_p$,
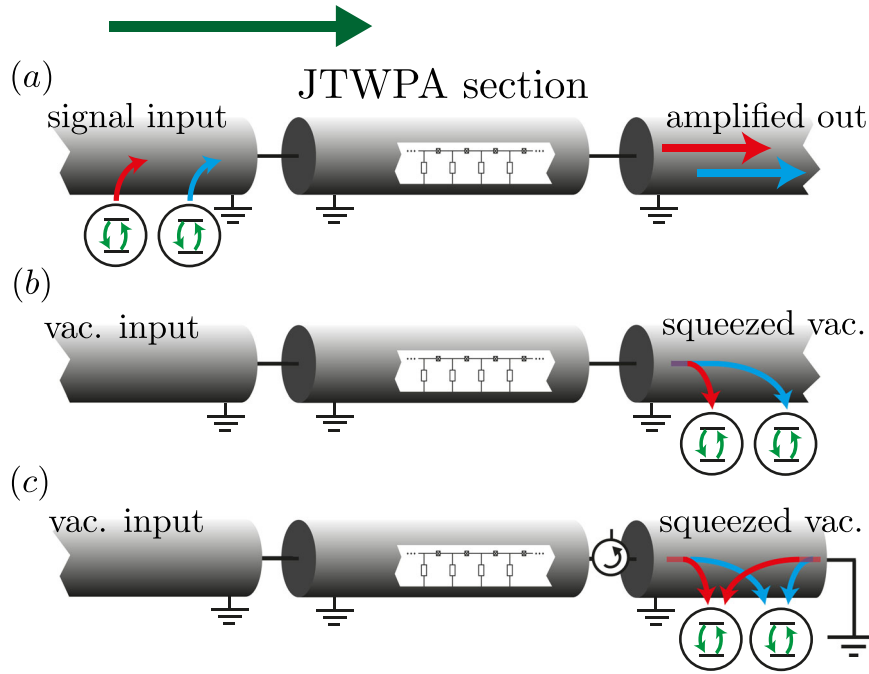
Fig. 6 Modes of operation for a JTPWA. **a** Amplification mode: quantum systems (here depicted as two-level systems to illustrate) are placed at the device input. **b** Probing mode: quantum systems placed at the output absorbs correlated photons from the JTWPA's output field and become entangled. **c** Reflection mode: higher degrees of entanglement can be reached by avoiding the left-moving vacuum noise. A circulator can be added to avoid back scattering into the JTWPA

the steady state of the two qubits is the product state $\rho = \rho_1 \otimes \rho_2$, where ρ_m is a thermal state with thermal population $N_R(\omega_m)/2$ and inversion $\langle \hat{\sigma}_z^{(m)} \rangle = -1/(N_R(\omega_m)+1)$. On the other hand, for $\omega_1 + \omega_2 = 2\Omega_p$ the qubits become entangled. Under the simplifying symmetric assumptions $N_R(\omega_m) \equiv N$ and $\gamma_m \equiv \gamma$ we find that

$$\left\langle \hat{\sigma}_x^{(1)} \hat{\sigma}_x^{(2)} \right\rangle = -\left\langle \hat{\sigma}_y^{(1)} \hat{\sigma}_y^{(2)} \right\rangle = \frac{\mathrm{Re}[M]}{\left[(N+1)(N+1)^2 - |M|^2 \right]}, \quad (7)$$

and

$$\left\langle \hat{\sigma}_x^{(1)} \hat{\sigma}_y^{(2)} \right\rangle = -\frac{\mathrm{Im}[M]}{\left[(N+1)(N+1)^2 - |M|^2 \right]}, \quad (8)$$

in steady state, where $M(\omega_i) \equiv M$. More general expressions are given in Supplementary Method 2. Hence, by measuring qubit–qubit correlation functions and single-qubit inversion using standard qubit readout protocols,[55–57] one can map out the squeezing spectrum of the source.

We can also turn this around and, rather than view the two qubits as a probe of the JTWPA's performance, view the JTWPA as a source of entanglement for the qubits. To achieve maximal degree of entanglement between the qubits, it is desirable to avoid the vacuum noise of the left-moving field. This can be achieved by squeezing the left-moving field with a separate JTWPA section, or more simply by operating the device in reflection mode, as illustrated in Fig. 6c.

Assuming ideal conditions where the qubits couple symmetrically to equally squeezed left-moving fields and right-moving fields, $N_L(\omega_i) = N_R(\omega_i) \equiv N/2$, $M_L(\omega_i) = M_R(\omega_i) \equiv M/2$, and an ideal lossless squeezing source, the steady state of the two qubits is the pure state (see Supplementary Method 2 for more information)

$$|\Psi^\theta\rangle = \frac{1}{\sqrt{2N+1}} \left(\sqrt{N+1}|gg\rangle + e^{i\theta}\sqrt{N}|ee\rangle \right), \quad (9)$$

where θ is the squeezing angle. For large N, this pure state approaches a maximally entangled state with
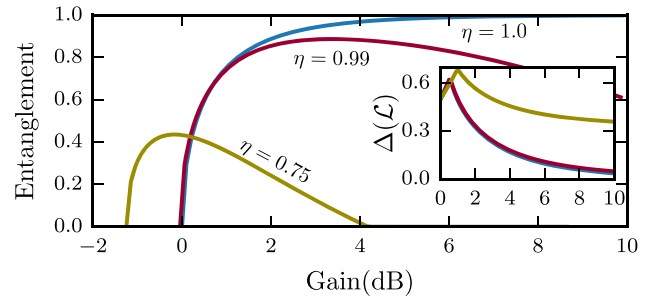

Fig. 7 Generating entanglement with squeezing. Concurrence of two qubits in a two-mode squeezed bath as a function of the gain of the squeezing source, $G(\omega,z) = \eta|u(\omega,z)|^2$, for three different source loss levels $\eta = 0.75, 0.99, 1.00$. No thermal noise at the squeezing source input is assumed. The inset shows the behavior of the spectral gap of the Lindbladian

entanglement entropy $E(|\Psi^\theta\rangle) = -\mathrm{tr}[\rho_1 \log_2(\rho_1)] \simeq 1 - 1/4N^2$, where $\rho_1 = \mathrm{tr}_2\left[|\Psi^\theta\rangle\langle\Psi^\theta|\right]$.

Of practical importance is the steady state entanglement's dependence on the degree of loss, and the behavior of the spectral gap of the Lindbladian in Eq. 34. The latter is important because it sets the time-scale for approaching the steady state. It is defined as $\Delta(\mathcal{L}) = |\mathrm{Re}\lambda_1|$, where λ_1 is the non-zero right-eigenvalue of $\mathcal{L}$ with real part closest to zero. In Fig. 7, we plot the steady state entanglement, quantified by the concurrence,[58] and the spectral gap as a function of gain for different values of η (as defined above). These results show that the achievable entanglement is very sensitive to loss, but an upshot is that relatively modest gains are needed to achieve high degree of entanglement.

CV cluster states

The two-qubit dynamics considered above demonstrates the JTWPA's potential for entanglement generation. To go beyond bi-

partite entanglement, one can add multiple pump tones, such that a single frequency can become entangled with multiple other "idler" frequencies in a multi-mode squeezed state, resulting in potentially complex patterns of entanglement. Together with its broadband nature and the potential for dispersion engineering, this turns the JTWPA into a powerful resource for dissipative quantum state preparation, as we demonstrate in the following.

To exemplify the potential of broadband squeezing as a resource for quantum computing and state preparation, we show below how CV cluster states can be generated through a dissipative and deterministic process, using the output field of multiple broadband squeezing sources. The cluster states are a powerful class of entangled many-body quantum states that are resource states for measurement-based quantum computing. Given a cluster state, an algorithm is executed using only single-site measurements and classical feed forward on the state.[59–63]

A CV cluster state is defined with respect to a (weighted) simple graph $G = (V, E)$, with V the set of vertices and E the set of edges. A CV quantum systems with quadratures $\hat{x}_v = (\hat{c}_v + \hat{c}_v^\dagger)/\sqrt{2}$ and $\hat{y}_v = -i(\hat{c}_v - \hat{c}_v^\dagger)/\sqrt{2}$, where $\hat{c}_v$ $(\hat{c}_v^\dagger)$ is a bosonic annihilation (creation) operator, is associated to each vertex v. The ideal CV cluster state (with respect to G) is defined as the unique state $|\phi_G\rangle$ satisfying[61, 63, 64]

$$\left(\hat{y}_v - \sum_{w \in \mathcal{N}(v)} a_{vw} \hat{x}_w \right) |\phi_G\rangle = 0 \quad \forall v \in V, \tag{10}$$

where $\mathcal{N}(v)$ is the neighborhood of v, i.e., all the vertices connected to v by an edge in E and $a_{vw} = a_{wv} \in [-1, 1]$ is the weight of the edge $\{v, w\}$. Note that $|\phi_G\rangle$ is an infinitely squeezed state, and thus not physical. In practice, one has to work with Gaussian states that approaches $|\phi_G\rangle$ in a limit of infinite squeezing. We can define an adjacency matrix $[a_{vw}]$ for the graph, where $a_{vw} = 0$ if there is no edge $\{v, w\} \in E$. Since the adjacency matrix uniquely defines the graph, and vice versa, we use the symbol G to interchangeably refer to both the graph and its adjacency matrix in the following.

We focus here on a class of graphs, first studied in refs 32, 33, satisfying two simplifying criteria: (1) The graph is bicolorable. This means that every vertex can be given one out of two colors, in such a way that every edge connects vertices of different colors (the square lattice is an example). (2) The graph's adjacency matrix is self-inverse, $G = G^{-1}$. The latter constraint has a simple geometric interpretation described in ref. 33. We show in Supplementary Method 3 that for a graph G satisfying these critera, the Lindblad equation $\dot{\rho} = \mathcal{L}_G \rho$, with Lindbladian

$$\mathcal{L}_G = \sum_{v \in V} \left\{ \kappa(N+1)\mathcal{D}[\hat{c}_v] + \kappa N \mathcal{D}[\hat{c}_v^\dagger] \right\}$$

$$- \sum_{\{v,w\} \in E} \kappa a_{vw} \mathcal{S}_{iM}[\hat{c}_v^\dagger, \hat{c}_w^\dagger], \tag{11}$$

where $M = \sqrt{N(N+1)}$ and $\mathcal{S}_{iM}[A, B]$ is defined in Eq. (35), has a unique steady state $|\phi_G(M)\rangle$ that approaches $|\phi_G\rangle$ as $M \to \infty$. The existence of graphs satisfying all the listed criteria, with associated cluster states, $|\phi_G\rangle$, that are universal for quantum computing is shown in refs 32, 33. Equation (11) is a remarkable result, because it implies that CV cluster states can be prepared simply by placing oscillators in a multi-mode squeezed bath, i.e., broadband squeezing is the only necessary resource for the preparation. In the following, we detail how multi-mode squeezed baths with an entanglement structure giving rise to universal cluster states can be engineered adapting a simple scheme from.[35]

In ref. 35, Wang and coworkers showed how cluster states with graphs of the type considered here could be generated through Hamiltonian interactions between the modes of optical parametric oscillators (OPOs), followed by an interferometer combining

modes from distinct OPOs. We adopt this scheme in the following, using JTWPAs (other types of broadband squeezing sources can also be used) in place of OPOs. The main difference between our proposal and that of ref 35 and previous proposals[32, 33] is that our scheme is purely dissipative: the CV modes of the cluster state never interact directly, but rather become entangled through absorption and stimulated emission of correlated photons from their environment. We focus primarily on a situation where the modes are embodied in multimode resonators, which is a particularly hardware efficient implementation. We emphasize, however, that due to the dissipative nature of the scheme, this is not a necessary constraint. The modes could in principle all be embodied in physically distinct and remote resonators, removing any constraints on locality. This is an attractive advantage of such a dissipative scheme.

Following ref. 35, the modes of the cluster states are resonator modes with equally spaced frequencies $\omega_m = \omega_0 + m\Delta$, where m is an integer, ω_0 is some frequency offset and Δ the frequency separation. We require a number of degenerate modes for each frequency ω_m: to create a D-dimensional cluster state requires a $2 \times D$-fold degeneracy per frequency. This can be achieved, e.g., by using $2 \times D$ identical multi-mode resonators, as illustrated for $D = 1$ in Fig. 8. Each resonator mode will be a vertex in the cluster state graph, and as will become clear below, a set of degenerate modes can be thought of as a graph "macronode".[35] It is convenient to relabel the frequencies with a "macronode index" $\mathcal{M} = (-1)^m m$.

We show in Supplementary Method 3 that a master equation with Lindbladian of the form Eq. (11) is realized for a single resonator interacting with a bath generated by the output field of a JTWPA with a single pump frequency $\Omega_p = \omega_0 + p\Delta/2$, where $p = m + n$ for some choice of frequencies $\omega_m \neq \omega_n$. The graph is in this case a trivial graph consisting of a set of disjoint pairs of vertices connected by an edge, i.e., a set of two-mode cluster states, which can be represented as $G_0 = $ •——• •——• •——• •——• … The edges have weight +1, under the assumption of a quantum limited, flat squeezing spectrum $M(\omega) = iM = i\sqrt{N(N+1)}$ with $N(\omega) = N$ over the relevant bandwidth.

More complex and useful graphs can be constructed using these two-mode cluster states as basic building blocks.[35] Taking a number of JTWPAs, each labeled by i and acting as a squeezing source independently generating a disjoint graph $G_i = $ •——• •——• •——• •——• … as above, universal cluster states can be created by combining the output fields of the different sources on an interferometer. The action of the interferometer can be written as a graph transformation, where $G = \oplus_i G_i$ transforms to $G \to RGR^T$, where $R = \oplus_{\mathcal{M}} R_D^{(\mathcal{M})}$ represents an interferometer acting independently on each macronode $\mathcal{M}$, i.e., each set of $2 \times D$-fold degenerate modes. R has to be orthogonal for the transformed graph to be self-inverse ($G = G^{-1}$), which we recall is one of the criteria for Eq. (11) to generate the corresponding cluster state. As shown in ref. 35 this is the case if the $2D \times 2D$ matrix R_D is a Hadamard transformation $R_D = H^{\otimes D}$ built from 2×2 Hadamard matrices

$$H = \frac{1}{\sqrt{2}} \begin{pmatrix} 1 & 1 \\ 1 & -1 \end{pmatrix}. \tag{12}$$

Physically such a transformation can be realized by pairwise interfering the output fields of the JTWPAs on 50-50 beam splitters with beam splitter matrix as in Eq. (12). The network of beam splitters needed for the case $D = 1$ is illustrated in Fig. 8, for $D = 2$ in Fig. 9, and for higher dimensions in ref. 35.

In ref. 35, it was shown that graphs G constructed in this way can give rise to D-dimensional cluster states that are universal for measurement-based quantum computing. Let us consider an
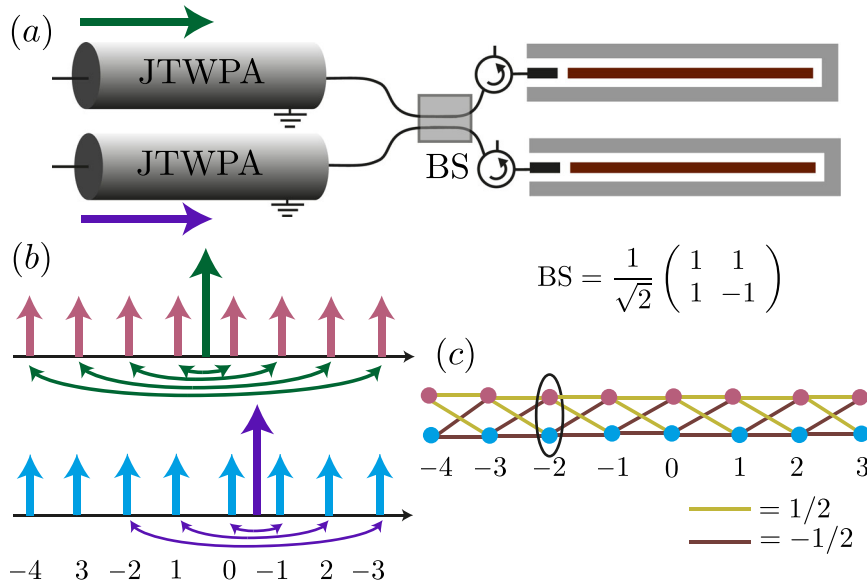
Fig. 8 Dissipative generation of a linear cluster state. **a** Two JTWPAs are used as squeezing sources. The output fields of the two devices are combined on a 50-50 beam splitter enacting a Hadamard transformation, before impinging on two identical multi-mode resonators. **b** Each JTWPA is pumped by a single pump tone, generating entanglement (*curved arrows*) between pairs of frequencies satisfying $\omega_n + \omega_m = 2\Omega_i$. We focus here on center frequencies corresponding to the frequencies of the resonator modes, illustrated by the *pink* and *blue arrows*. The numbers show the macronode index of each frequency. **c** Linear graph defining the steady state cluster state of the resonator modes. The horizontal edges are generated by the two pumps, while the diagonal edges are generated by the Hadamard transformation (see Supplementary Method 3 for details). The numbers show the macronode index, and the *circle* shows macronode $\mathcal{M} = -2$ in the graph

example with $D = 1$ in some more detail to illustrate the basic principles. First, take two JTWPAs pumped individually with respective pump frequencies Ω_i and Ω_j, with $i = -j = \Delta\mathcal{M}$. On the macronode level, this gives exactly one edge between macronodes separated by $|\Delta\mathcal{M}|$, as illustrated by the horizontal edges in Fig. 8 for $\Delta\mathcal{M} = 1$. By interfering the output fields of the two JTWPAs on a beam splitter defined by Eq. (12), every node in each macronode becomes entangled with every node in the neighboring macronode, as illustrated by the diagonal edges in the figure. This gives a graph G with a linear structure, corresponding to a one-dimensional cluster state that is universal for single-mode quantum computation.[33–35]

The scheme can straight-forwardly be scaled up to arbitrary D-dimensional cluster states using $2 \times D$ squeezing sources and the same number of beam splitter transformations as shown in ref. 35. $D = 2$ is sufficient for universal quantum computation; a possible setup of JTWPAs and resonators is illustrated in Fig. 9. As emphasized in ref. 35, the relative ease of creating even higher dimensional cluster states is a very attractive property of the scheme.

DISCUSSION
We have shown how the recently developed JTWPAs are powerful sources of nonclassical radiation. The design flexibility and broad bandwidth allows us to tailor the properties of the quantum radiation emitted by the device through dispersion engineering. In this way, the output field can be optimized for specific applications where broadband squeezing is useful. Furthermore, we have illustrated how the output field of one or multiple JTWPAs can be used for reservoir engineering: By placing quantum systems at the output of a broadband squeezing source, the systems can be driven into non-trivial entangled states through correlated photon absorption and emission processes. We have shown both how to prepare pairs of entangled qubits, as well as CV cluster states that are universal for quantum computing in this manner.
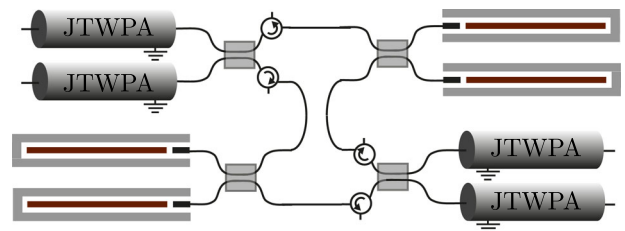

Fig. 9 Schematic setup for a universal microwave quantum computer. Four JTWPAs are used as squeezing sources to dissipatively prepare the modes of four identical multi-mode resonators in a two-dimensional cluster state. The quantum computation is subsequently performed through Gaussian and non-Gaussian (e.g., photon-number resolving[78]) single-mode measurements on the resonators.[63]

Moreover, a JTWPA can be thought of as an artificial non-linear crystal, introducing a new non-linear element to the field of microwave quantum optics. The JTWPA is qualitatively different from previous, essentially point-like, non-linear elements used in microwave circuits and represents, in this respect, a major departure from the conventional paradigm of "circuit quantum electrodynamics" based on localized electromagnetic modes.[55] The possibility of dispersion engineering together with controllable non-linear parametric interactions opens new possibilities for quantum optics in the microwave regime, for example studying the interplay between light and matter in structured non-linear media.[65, 66]

METHODS
Asymptotic input–output theory
As shown in Supplementary Methods 1, the position-dependent flux, $\hat{\phi}(x)$ (in the Schrödinger picture), along a transmission line with a JTWPA section extending from $x = 0$ to $x = z$ can in the continuum limit be

expanded in terms of a set of left-moving modes and right-moving modes,

$$\hat{\phi}(x) = \sum_{\nu=\mathrm{L,R}} \int_0^\infty d\omega \sqrt{\frac{\hbar}{2c(x)\omega}} g_{\nu\omega}(x) \hat{a}_{\nu\omega} + \mathrm{H.c.,} \qquad (13)$$

where $\left[\hat{a}_{\nu\omega}, \hat{a}_{\mu\omega'}^\dagger\right] = \delta_{\nu\mu}\delta(\omega - \omega')$ and the mode functions are given by

$$g_{\nu\omega}(x) = \sqrt{\frac{1}{2\pi\eta_\omega(x)v(x)}} e^{\pm ik_\omega(x)x}. \qquad (14)$$

Here, $+$ ($-$) corresponds to $\nu = \mathrm{R}$ ($\nu = \mathrm{L}$), $k_\omega(x) = \eta_\omega(x)\omega/v(x)$ is the wavevector, with $\eta_\omega(x)$ the refractive index, and $v(x) = 1/\sqrt{c(x)l(x)}$. The x-dependent parameters are defined such that they take one (constant) value inside the JTWPA section, and another value outside this section. We have defined $c(x)$, the capacitance to ground per unit cell, and $l(x)$, the linear inductance of the transmission line. We emphasize that this simple form of the mode functions assumes that we can neglect reflection at the interfaces between the JTWPA and the linear transmission line sections.[48]

The only difference from the usual prescription for the quantized flux in a linear, homogeneous and dispersion free transmission line[67, 68] is the x-dependent wavevector, which now takes a different form inside and outside the nonlinear section. Explicitly, the dispersion relation is found to be (see Supplementary Methods 1 and ref. 9)

$$k_\omega(x) = \begin{cases} \sqrt{\dfrac{-i\omega z^{-1}(\omega)l(x)}{1 - \omega^2/\omega_\mathrm{P}^2}} & \text{for } 0 < x < z \\[2em] \dfrac{\omega}{v(x)} & \text{otherwise,} \end{cases} \qquad (15)$$

where $z^{-1}(\omega) = Z^{-1}(\omega)/a$ is the admittance to ground per unit cell in the JTWPA section.

Implicit in the continuum description is that we are considering sufficiently low frequencies, such that the wavelengths are large compared to the unit cell distance, a. Furthermore, plane wave solutions only exists when the right hand side of Eq. (15) is real. In practice, we are interested in frequencies $\omega^2 \ll \omega_\mathrm{P}^2$ such that the dispersion due to the plasma oscillations of the junctions is relatively small. If, however, the admittance $z^{-1}(\omega)$ describes a linear element with a resonant mode, a bandgap opens around the resonance frequency for which no plane wave solutions exists. Physically, such a resonant mode behaves as a "matter field" in the continuum limit, and the excitations of the systems resemble light-matter polaritons.[69–71] As long as we are away from any bandgap, however, these "matter fields" slave the photonic field, $\hat{\phi}(x, t)$, and only modifies the dielectric properties of the medium, manifest in the dispersion relation Eq. (15).

We assume the presence of a strong right-moving classical pump centered at a frequency Ω_P with corresponding wavevector k_p, and replace $\hat{a}_{R\omega} \to \hat{a}_{R\omega} + b(\omega)$, with $b(\omega)$ a complex valued function centered at Ω_P. The fields, $\hat{a}_{\nu\omega}$, are assumed to be sufficiently weak so that we can drop in $\hat{H}_1$ terms that are smaller than second order in the pump. As shown in Supplementary Methods 1, a Hamiltonian for the system can then be found of the form $\hat{H} = \hat{H}_0 + \hat{H}_1$ where $\hat{H}_0$ and $\hat{H}_1$ are given in Eqs. (1) and (2), respectively, with

$$\hat{H}_\mathrm{CPM} = -\frac{\hbar}{2\pi} \int_0^\infty d\omega d\omega' d\Omega d\Omega' \sqrt{k_\omega k_{\omega'}} \beta^*(\Omega)\beta(\Omega') \qquad (16)$$

$$\times \Phi(\omega, \omega', \Omega, \Omega') \hat{a}_{R\omega}^\dagger \hat{a}_{R\omega'} + \mathrm{H.c.,}$$

describing cross-phase modulation,

$$\hat{H}_\mathrm{SQ} = -\frac{\hbar}{4\pi} \int_0^\infty d\omega d\omega' d\Omega d\Omega' \sqrt{k_\omega k_{\omega'}} \beta(\Omega)\beta(\Omega') \qquad (17)$$

$$\times \Phi(\omega, \Omega, \omega', \Omega') \hat{a}_{R\omega}^\dagger \hat{a}_{R\omega'}^\dagger + \mathrm{H.c.,}$$

describing broadband squeezing, and

$$H_\mathrm{SPM} = -\frac{\hbar}{4\pi} \int_0^\infty d\omega d\omega' d\Omega d\Omega' \sqrt{k_\omega k_{\omega'}} \beta^*(\Omega)\beta(\Omega') \qquad (18)$$

$$\times \Phi(\omega, \omega', \Omega, \Omega') b^*(\omega)b(\omega') + \mathrm{H.c.,}$$

describing self-phase modulation of the pump. Here we have furthermore

dropped fast rotating terms and the highly phase mismatched left moving field.

For notational convenience, we have defined the phase matching function[72, 73]

$$\Phi(\omega_1, \omega_2, \omega_3, \omega_4) = \int_0^z dx e^{-i\left[k_{\omega_1}(x) - k_{\omega_2}(x) + k_{\omega_3}(x) - k_{\omega_4}(x)\right]x}, \qquad (19)$$

and a dimensionless pump amplitude, $\beta(\Omega)$, which as shown in Supplementary Methods 1, can be written in terms of the ratio of the pump current to the Josephson junction critical current,

$$\beta(\Omega) = \frac{I_\mathrm{p}(\Omega)}{4I_\mathrm{c}}, \qquad (20)$$

where $I_\mathrm{c} = (2\pi/\Phi_0)E_J$.

It should be noted that $\hat{H}_1$ can also in principle include frequency conversion processes where a photon with frequency close to $2\Omega_\mathrm{p} + \omega$ is created by absorbing a single photon at frequency ω and two pump photons at Ω_p. We have left out such contributions in Eq. (2) under the assumption that appropriate steps have been taken to ensure that these frequency conversion processes are heavily phase mismatched. In particular, current experiments use low-pass filters before and after entry to the JTWPA section of the transmission line, which ensures that no plane-wave solutions exist above $2\Omega_p$ [Gustavsson, S. & Krantz, P. Private communication (2016)].

The dynamics according to the non-linear Hamiltonian $\hat{H}_1$ is in general difficult to treat analytically to all orders,[72, 73] and we therefore take a perturbative approach treating the non-linearity to first order. An input–output relation linking the field entering the JTWPA to the emitted output field can then be derived in the usual asymptotic scattering limit.[71–75] Equations of motion similar to those we derive here have been used previously by Caves and Crouch in a study of wideband traveling wave amplifier,[49] where they were taken as operator versions of macroscopic Maxwell's equations for a nonlinear, homogeneous and dispersionless medium.[76] We here justify similar input–output relations by deriving them from a microscopic theory, taking into account the finite extent of the nonlinearity as well as dispersion. For the JTWPA the latter stems from both junction plasma oscillations, non-linear phase-modulation and engineered bandgaps in the medium.

Treating $\hat{H}_1$ as a perturbation, it is natural to go to an interaction picture with respect to $\hat{H}_0$. The time-evolution operator for the problem in this picture is

$$\hat{U}(t_0, t_1) = \mathcal{T} e^{-\frac{i}{\hbar} \int_{t_0}^{t_1} dt \hat{H}_1(t)}, \qquad (21)$$

where $\hat{H}_1(t) = \exp\left[(i/\hbar)\hat{H}_0 t\right] \hat{H}_1 \exp\left[-(i/\hbar)\hat{H}_0 t\right]$ and $\mathcal{T}$ is the time-ordering operator.

Solving the time-dynamics according to Eq. (21) is difficult in general. However, if we neglect any backaction from the fields onto the pump, i.e., take the undepleted pump approximation and disregard any quantum fluctuations around the pump frequency, we can solve for the pump separately according to the classical Hamiltonian H_SPM and substitute this back into the remaining parts of $\hat{H}_1$. The remainder is then effectively a quadratic Hamiltonian for the quantum fields. We will in the following also make several further simplifications that greatly reduces the complexity of the problem. First of all, we treat $\hat{H}_1$ as a perturbation to first order only, in which case the time-ordering in Eq. (21) can be dropped. See, however, refs 72, 73 for a discussion on the breakdown of this approximation. Subsequently we take a "scattering limit" and let the initial and final times go to $t_0 = -\infty$ and $t_1 = \infty$, respectively. The time-integral then gives rise to delta-functions in frequency space, and we are left with approximate asymptotic evolution operator, or scattering matrix,[71]

$$\hat{U} \equiv \hat{U}(-\infty, \infty) = e^{-\frac{i}{\hbar}\hat{K}_1}, \qquad (22)$$

where

$$\hat{K}_1 = \hat{K}_\mathrm{CPM} + \hat{K}_\mathrm{SQ} + K_\mathrm{SPM}. \qquad (23)$$

Explicit expressions for $\hat{K}_1$ for a general classical pump can be found in Supplementary Methods 1. We from now on make one last simplifying approximation and focus on the monochromatic pump limit, taking $b(\omega) \to b(\omega)\delta(\omega - \Omega_\mathrm{p})$. In this limit we have

$$\hat{K}_\mathrm{CPM} = -2\hbar z \int_0^\infty d\omega |\beta|^2 k_\omega \hat{a}_{R\omega}^\dagger \hat{a}_{R\omega}, \qquad (24)$$

and

$$\hat{K}_{SQ} = -\frac{\hbar}{2} \int_0^\infty d\omega \lambda(\omega) \Phi[-\Delta k_L(\omega)] \times \hat{a}_{R\omega}^\dagger \hat{a}_{R(2\Omega_p - \omega)}^\dagger + \text{H.c.}, \quad (25)$$

and $K_{SPM} = -\hbar z |\beta|^2 k_p b_p^* b_p$, where we have defined $b_p = b(\Omega_p)$, $\beta = \beta(\Omega_p)$ and

$$\lambda(\omega) = \beta^2 \sqrt{k_\omega k_{2\Omega_p - \omega}}, \quad (26)$$

$$\Delta k_L(\omega) = 2k_p - k_\omega - k_{2\Omega_p - \omega}. \quad (27)$$

Here, $\Delta k_L(\omega)$ quantifies a phase-mismatch due to the linear dispersion in the JTWPA section. As we show below there is also an additional nonlinear contribution to the phase-mismatch that must be taken into account.

Defining asymptotic output fields, $\hat{a}_{R\omega}^{out} = \hat{U}^\dagger \hat{a}_{R\omega} \hat{U}$, we find the input–output relation in Eq. (3), where

$$u(\omega, z) = \cosh[g(\omega)z] - \frac{i\Delta k(\omega)}{2g(\omega)} \sinh[g(\omega)z], \quad (28)$$

$$v(\omega, z) = \frac{\lambda(\omega)}{g(\omega)} \sinh[g(\omega)z], \quad (29)$$

$$g(\omega) = \sqrt{|\lambda(\omega)|^2 - \left(\frac{\Delta k(\omega)}{2}\right)^2}. \quad (30)$$

A straightforward calculation shows that $|u(\omega, z)|^2 - |v(\omega, z)|^2 = 1$, and that the modes satisfy the commutation relation $[\hat{a}_{R\omega}^{out}, \hat{a}_{R\omega'}^{out\dagger}] = \delta(\omega - \omega')$.

To summarize, this limiting equation is valid for weak nonlinearity and weak fields, only treating the nonlinear Hamiltonian $\hat{H}_1$ to first order, a strong monochromatic classical pump at a frequency Ω_p, and in an asymptotic large time limit where $t_0 = -\infty$ and $t_1 = \infty$.

How can we interpret the asymptotic limit where the initial and final times are taken to minus and plus infinity, respectively? If we consider a situation where an initial wave packet is localized far away at $x \ll 0$ at an early time $t_0 \ll 0$, this can be interpreted as a scattering limit, where we let the wave packet propagate through the nonlinearity and consider the asymptotic field at $x \gg z$ for a late time $t_1 \gg 0$.[71, 75] Since the initial evolution before the wave packet enters the nonlinear section is governed by $\hat{H}_0$, it is trivial to propagate the wave packet forward towards the nonlinearity. The late evolution after the wave packet has left the nonlinear section is similarly trivial. We can therefore think of $\hat{a}_{R\omega}$ as a frequency domain input field entering the JTWPA and $\hat{a}_{R\omega}^{out}$ as the corresponding output field leaving the device. This is similar to the definition of input and output fields used in the description of damped quantum optical systems.[75, 77] One should keep in mind, however, that the validity of this interpretation depends on the problem one is trying to solve: it is clearly not appropriate if, for example, the initial state of the field is delocalized over the nonlinear section.

The squeezing spectrum

The squeezing of the JTWPA's output field is manifest in correlations between frequencies ω and $2\Omega_p - \omega$, symmetric around the pump frequency. It is convenient to define for the right moving field the thermal photon number

$$N_R(\omega, z) = \int_0^\infty d\omega' \left\{ \langle \hat{a}_{R\omega}^{out\dagger} \hat{a}_{R\omega'}^{out} \rangle - \langle \hat{a}_{R\omega}^{out\dagger} \rangle \langle \hat{a}_{R\omega'}^{out} \rangle \right\}, \quad (31)$$

the squeezing parameter

$$M_R(\omega, z) = \int_0^\infty d\omega' \left\{ \langle \hat{a}_{R\omega}^{out} \hat{a}_{R\omega'}^{out} \rangle - \langle \hat{a}_{R\omega}^{out} \rangle \langle \hat{a}_{R\omega'}^{out} \rangle \right\}, \quad (32)$$

and the squeezing spectrum[50]

$$S_R(\omega, z) = \int_0^\infty d\omega' \langle \Delta \hat{Y}_{R\omega}^\theta \Delta \hat{Y}_{R\omega'}^\theta \rangle, \quad (33)$$

$$= 2N_R(\omega, z) + 1 - 2|M_R(\omega, z)|$$

where we have defined quadratures $\hat{Y}_{R\omega}^\theta = i[e^{i\theta/2} \hat{a}_{R\omega}^{out\dagger} - e^{-i\theta/2} \hat{a}_{R\omega}^{out}]$, with fluctuations $\Delta \hat{Y}_{R\omega} = \hat{Y}_{R\omega} - \langle \hat{Y}_{R\omega} \rangle$. We have also defined θ, the squeezing angle, which is given through $M_R(\omega, z) = |M_R(\omega, z)| e^{i\theta}$. We emphasize that Eqs. (31)–(33) are defined exclusively in terms of the right-moving field. The left-moving field also contributes vacuum noise and might add to the total photon number, but will have zero squeezing parameter in the absence of left-moving pump fields. The squeezing spectrum is typically probed in experiments by heterodyne measurement of filtered field quadratures.[43, 52–54] We discuss how Eq. (33) is probed in some more detail in Supplementary Methods 1.

For a vacuum input field, where $\langle \hat{a}_R(\omega, 0) \hat{a}_R^\dagger(\omega', 0) \rangle = \delta(\omega - \omega')$ and all other second order moments vanish, it follows that $N_R(\omega, z) = G(\omega, z) - 1 = |v(\omega, z)|^2$ and $M_R(\omega, z) = iu(\omega, z)v(\omega, z)e^{i\Delta k(\omega)z}$. These expressions satisfy $|M_R(\omega, z)|^2 = N_R(\omega, z)[N_R(\omega, z) - 1]$, the maximum value allowed by the Heisenberg uncertainty relation and also imply quantum-limited amplification.[13] This, of course, assumes that there is no internal loss in the JTWPA device.

Two qubits in a squeezed bath

Assuming for simplicity that the qubits are both located at the JTWPA output, $x_0 > z$, their reduced dynamics after tracing out the bath is governed by a Markovian master equation, $\dot{\rho} = \mathcal{L}\rho$. The form of $\mathcal{L}$ for the general case is given in Supplementary Method 2, while we here focus on the most interesting situation when the two qubits are tuned in with the squeezing interaction, such that $\omega_1 + \omega_2 = 2\Omega_p$. We can then write the Lindbladian in the interaction picture

$$\mathcal{L} = \sum_{\substack{\nu = L,R \\ m=1,2}} \left\{ \frac{\gamma_m}{2}(N_{m,\nu} + 1)\mathcal{D}[\hat{\sigma}_-^{(m)}] + \frac{\gamma_m}{2}N_{m,\nu}\mathcal{D}[\hat{\sigma}_+^{(m)}] \right\}$$
$$- \frac{\sqrt{\gamma_1\gamma_2}}{2}\mathcal{S}_{M_\nu}[\hat{\sigma}_+^{(1)}, \hat{\sigma}_+^{(2)}], \quad (34)$$

where

$$\mathcal{S}_M[A, B]\rho = M(A\rho B + B\rho A - \{AB, \rho\}) + \text{H.c.}, \quad (35)$$

describes a dissipative squeezing interaction, and $\mathcal{D}[A]\rho = A\rho A^\dagger - \{A^\dagger A, \rho\}/2$ is the usual dissipator. γ_m is the decay rate of qubit m and $\hat{\sigma}_- = |g\rangle\langle e|$ ($\hat{\sigma}_+ = |e\rangle\langle g|$) is the qubit lowering (raising) operator. The Lindbladian has two contributions coming from the left-moving and the right-moving field, respectively. In general, both fields can have non-zero thermal photon number $N_{m,\nu} = N_\nu(\omega_m)$ and squeezing parameter $M_\nu = [M_\nu(\omega_1) + M_\nu(\omega_2)]/2$. If, on the other hand, the qubits are tuned out of resonance with the squeezing interaction, $\omega_1 + \omega_2 \neq 2\Omega_p$, the last line in Eq. (34) will be fast rotating and can be dropped in a rotating wave approximation (see Supplementary Method 3 for more details).

AUTHOR CONTRIBUTIONS

All authors conceptualized the project. A.L.G. proposed to use JTWPAs to generate cluster states and worked through the detailed calculations. A.L.G. wrote the manuscript with contributions from A.B.

REFERENCES

1. Frey, T. et al. Dipole coupling of a double quantum dot to a microwave resonator. *Phys. Rev. Lett.* **108**, 046807 (2012).
2. Kubo, Y. et al. Strong coupling of a spin ensemble to a superconducting resonator. *Phys. Rev. Lett.* **105**, 140502 (2010).
3. Wallraff, A. et al. Strong coupling of a single photon to a superconducting qubit using circuit quantum electrodynamics. *Nature* **431**, 162–167 (2004).
4. Paik, H. et al. Observation of high coherence in josephson junction qubits measured in a three-dimensional circuit qed architecture. *Phys. Rev. Lett.* **107**, 240501 (2011).

5. Astafiev, O. et al. Resonance fluorescence of a single artificial atom. *Science* **327**, 840–843 (2010).

6. Van Loo, A. F. et al. Photon-mediated interactions between distant artificial atoms. *Science* **342**, 1494–1496 (2013).

7. Niemczyk, T. et al. Circuit quantum electrodynamics in the ultrastrong-coupling regime. *Nat. Phys.* **6**, 772–776 (2010).

8. Wilson, C. et al. Observation of the dynamical casimir effect in a superconducting circuit. *Nature* **479**, 376–379 (2011).

9. O'Brien, K., Macklin, C., Siddiqi, I. & Zhang, X. Resonant phase matching of josephson junction traveling wave parametric amplifiers. *Phys. Rev. Lett.* **113**, 157001 (2014).

10. Macklin, C. et al. A near–quantum-limited josephson traveling-wave parametric amplifier. *Science* **350**, 307–310 (2015).

11. White, T. et al. Traveling wave parametric amplifier with josephson junctions using minimal resonator phase matching. *Appl. Phys. Lett.* **106**, 242601 (2015).

12. Hillery, M. *Quantum squeezing* Ch. 2 (Springer, 2004).

13. Caves, C. M. Quantum limits on noise in linear amplifiers. *Phys. Rev. D* **26**, 1817–1839 (1982).

14. Jeffrey, E. et al. Fast accurate state measurement with superconducting qubits. *Phys. Rev. Lett.* **112**, 190504 (2014).

15. Castellanos-Beltran, M. & Lehnert, K. Widely tunable parametric amplifier based on a superconducting quantum interference device array resonator. *Appl. Phys. Lett.* **91**, 083509 (2007).

16. Bergeal, N. et al. Phase-preserving amplification near the quantum limit with a josephson ring modulator. *Nature* **465**, 64–68 (2010).

17. Hatridge, M., Vijay, R., Slichter, D. H., Clarke, J. & Siddiqi, I. Dispersive magnetometry with a quantum limited squid parametric amplifier. *Phys. Rev. B.* **83**, 134501 (2011).

18. Caves, C. M., Combes, J., Jiang, Z. & Pandey, S. Quantum limits on phase-preserving linear amplifiers. *Phys. Rev. A* **86**, 063802 (2012).

19. Palma, G. M. & Knight, P. L. Phase-sensitive population decay: the two-atom dicke model in a broadband squeezed vacuum. *Phys. Rev. A* **39**, 1962–1969 (1989).

20. Gómez, A. V., Rodrguez, F. J., Quiroga, L. & Garca-Ripoll, J. J. Entangled microwaves as a resource for entangling spatially separate solid-state qubits: superconducting qubits, nv centers and magnetic molecules. Preprint at arXiv:1512.00269 (2015).

21. Furusawa, A. et al. Unconditional quantum teleportation. *Science* **282**, 706–709 (1998).

22. Yurke, B., McCall, S. L. & Klauder, J. R. Su(2) and su(1,1) interferometers. *Phys. Rev. A* **33**, 4033–4054 (1986).

23. Tsang, M. & Caves, C. M. Evading quantum mechanics: engineering a classical subsystem within a quantum environment. *Phys. Rev. X* **2**, 031016 (2012).

24. Barzanjeh, S., DiVincenzo, D. P. & Terhal, B. M. Dispersive qubit measurement by interferometry with parametric amplifiers. *Phys. Rev. B* **90**, 134515 (2014).

25. Didier, N., Kamal, A., Oliver, W. D., Blais, A. & Clerk, A. A. Heisenberg-limited qubit read-out with two-mode squeezed light. *Phys. Rev. Lett.* **115**, 093604 (2015).

26. Royer, B., Grimsmo, A. L., Didier, N. & Blais, A. Fast and high-fidelity entangling gate through parametrically modulated longitudinal coupling. Preprint at arXiv:1603.04424 (2016).

27. Ong, F. R. et al. Quantum heating of a nonlinear resonator probed by a superconducting qubit. *Phys. Rev. Lett.* **110**, 047001 (2013).

28. Aharonov, D. et al. Adiabatic quantum computation is equivalent to standard quantum computation. *SIAM Rev.* **50**, 755–787 (2008).

29. Nielsen, M. A. & Chuang, I. L. *Quantum computation and quantum information*, (Cambridge university press, 2010).

30. Verstraete, F., Wolf, M. M. & Cirac, J. I. Quantum computation and quantum-state engineering driven by dissipation. *Nat. Phys.* **5**, 633–636 (2009).

31. Kraus, B. et al. Preparation of entangled states by quantum markov processes. *Phys. Rev. A* **78**, 042307 (2008).

32. Menicucci, N. C., Flammia, S. T. & Pfister, O. One-way quantum computing in the optical frequency comb. *Phys. Rev. Lett.* **101**, 130501 (2008).

33. Flammia, S. T., Menicucci, N. C. & Pfister, O. The optical frequency comb as a one-way quantum computer. *J. Phys. B At. Mol. Opt. Phys.* **42**, 114009 (2009).

34. Menicucci, N. C. Temporal-mode continuous-variable cluster states using linear optics. *Phys. Rev. A* **83**, 062314 (2011).

35. Wang, P., Chen, M., Menicucci, N. C. & Pfister, O. Weaving quantum optical frequency combs into continuous-variable hypercubic cluster states. *Phys. Rev. A* **90**, 032325 (2014).

36. Chen, M., Menicucci, N. C. & Pfister, O. Experimental realization of multipartite entanglement of 60 modes of a quantum optical frequency comb. *Phys. Rev. Lett.* **112**, 120505 (2014).

37. Alexander, R. N. et al. One-way quantum computing with arbitrarily large time-frequency continuous-variable cluster states from a single optical parametric oscillator. Preprint at arXiv:1509.00484 (2015).

38. Brecht, T. et al. Multilayer microwave integrated quantum circuits for scalable quantum computing. *Npj Quant. Inf.* **2**, 16002 (2016).

39. Eom, B. H., Day, P. K., LeDuc, H. G. & Zmuidzinas, J. A wideband, low-noise superconducting amplifier with high dynamic range. *Nat. Phys.* **8**, 623–627 (2012).

40. Bockstiegel, C. et al. Development of a broadband nbtin traveling wave parametric amplifier for mkid readout. *J. Low Temp. Phys.* **176**, 476–482 (2014).

41. Roy, T. et al. Broadband parametric amplification with impedance engineering: beyond the gain-bandwidth product. *Appl. Phys. Lett.* **107**, 262601 (2015).

42. Metelmann, A. & Clerk, A. A. Quantum-limited amplification via reservoir engineering. *Phys. Rev. Lett.* **112**, 133904 (2014).

43. Forgues, J.-C., Lupien, C. & Reulet, B. Experimental violation of bell-like inequalities by electronic shot noise. *Phys. Rev. Lett.* **114**, 130403 (2015).

44. Grimsmo, A. L., Qassemi, F., Reulet, B. & Blais, A. Quantum optics theory of electronic noise in coherent conductors. *Phys. Rev. Lett.* **116**, 043602 (2016).

45. Yaakobi, O., Friedland, L., Macklin, C. & Siddiqi, I. Parametric amplification in josephson junction embedded transmission lines. *Phys. Rev. B* **87**, 144301 (2013).

46. Bell, M. T. & Samolov, A. Traveling-wave parametric amplifier based on a chain of coupled asymmetric squids. *Phys. Rev. Appl.* **4**, 024014 (2015).

47. Zorin, A. Traveling-wave parametric amplifier with three-wave mixing in superconducting transmission line with embedded rf-squids. Preprint at arXiv:1602.02650 (2016).

48. Santos, D. J. & Loudon, R. Electromagnetic-field quantization in inhomogeneous and dispersive one-dimensional systems. *Phys. Rev. A* **52**, 1538–1549 (1995).

49. Caves, C. M. & Crouch, D. D. Quantum wideband traveling-wave analysis of a degenerate parametric amplifier. *J. Opt. Soc. Am. B* **4**, 1535–1545 (1987).

50. Wustmann, W. & Shumeiko, V. Parametric resonance in tunable superconducting cavities. *Phys. Rev. B* **87**, 184501 (2013).

51. Mallet, F. et al. Quantum state tomography of an itinerant squeezed microwave field. *Phys. Rev. Lett.* **106**, 220502 (2011).

52. Eichler, C. et al. Observation of two-mode squeezing in the microwave frequency domain. *Phys. Rev. Lett.* **107**, 113601 (2011).

53. Flurin, E., Roch, N., Mallet, F., Devoret, M. H. & Huard, B. Generating entangled microwave radiation over two transmission lines. *Phys. Rev. Lett.* **109**, 183901 (2012).

54. Eichler, C., Salathe, Y., Mlynek, J., Schmidt, S. & Wallraff, A. Quantum-limited amplification and entanglement in coupled nonlinear resonators. *Phys. Rev. Lett.* **113**, 110502 (2014).

55. Blais, A., Huang, R.-S., Wallraff, A., Girvin, S. M. & Schoelkopf, R. J. Cavity quantum electrodynamics for superconducting electrical circuits: an architecture for quantum computation. *Phys. Rev. A* **69**, 062320 (2004).

56. Vijay, R., Slichter, D. H. & Siddiqi, I. Observation of quantum jumps in a superconducting artificial atom. *Phys. Rev. Lett.* **106**, 110502 (2011).

57. Jeffrey, E. et al. Fast accurate state measurement with superconducting qubits. *Phys. Rev. Lett.* **112**, 190504 (2014).

58. Wootters, W. K. Entanglement of formation and concurrence. *Quant. Inf. Comput.* **1**, 27–44 (2001).

59. Raussendorf, R. & Briegel, H. J. A one-way quantum computer. *Phys. Rev. Lett.* **86**, 5188 (2001).

60. Raussendorf, R., Browne, D. E. & Briegel, H. J. Measurement-based quantum computation on cluster states. *Phys. Rev. A* **68**, 022312 (2003).

61. Menicucci, N. C. et al. Universal quantum computation with continuous-variable cluster states. *Phys. Rev. Lett.* **97**, 110501 (2006).

62. Briegel, H. J., Browne, D. E., Dür, W., Raussendorf, R. & Van den Nest, M. Measurement-based quantum computation. *Nat. Phys.* **5**, 19–26 (2009).

63. Gu, M., Weedbrook, C., Menicucci, N. C., Ralph, T. C. & van Loock, P. Quantum computing with continuous-variable clusters. *Phys. Rev. A.* **79**, 062318 (2009).

64. Menicucci, N. C., Flammia, S. T. & van Loock, P. Graphical calculus for gaussian pure states. *Phys. Rev. A* **83**, 042335 (2011).

65. Joannopoulos, J. D., Johnson, S. G., Winn, J. N. & Meade, R. D. *Photonic Crystals: Molding The Flow Of Light*, (Princeton university press, 2011).

66. Douglas, S. et al. Quantum many-body models with cold atoms coupled to photonic crystals. *Nat. Photon.* **9**, 326–331 (2015).

67. Yurke, B. & Denker, J. S. Quantum network theory. *Phys. Rev. A* **29**, 1419–1437 (1984).

68. Yurke, B. *Quantum Squeezing* Ch. 3 (Springer, 2004).

69. Huttner, B., Baumberg, J. & Barnett, S. Canonical quantization of light in a linear dielectric. *Europhys. Lett.* **16**, 177 (1991).

70. Huttner, B. & Barnett, S. M. Quantization of the electromagnetic field in dielectrics. *Phys. Rev. A* **46**, 4306–4322 (1992).

71. Drummond, P. D. & Hillery, M. *The Quantum Theory Of Nonlinear Optics*, (Cambridge University Press, 2014).

72. Quesada, N. & Sipe, J. E. Effects of time ordering in quantum nonlinear optics. *Phys. Rev. A* **90**, 063840 (2014).

73. Quesada, N. & Sipe, J. E. Time-ordering effects in the generation of entangled photons using nonlinear optical processes. *Phys. Rev. Lett.* **114**, 093903 (2015).

74. Breit, G. & Bethe, H. A. Ingoing waves in final state of scattering problems. *Phys. Rev.* **93**, 888–890 (1954).

75. Liscidini, M., Helt, L. G. & Sipe, J. E. Asymptotic fields for a hamiltonian treatment of nonlinear electromagnetic phenomena. *Phys. Rev. A* **85**, 013833 (2012).

76. Hillery, M. & Mlodinow, L. D. Quantization of electrodynamics in nonlinear dielectric media. *Phys. Rev. A* **30**, 1860–1865 (1984).

77. Gardiner, C. W. & Collett, M. J. Input and output in damped quantum systems: Quantum stochastic differential equations and the master equation. *Phys. Rev. A* **31**, 3761 (1985).

78. Schuster, D. et al. Resolving photon number states in a superconducting circuit. *Nature* **445**, 515–518 (2007).